Int. J. Heat Mass Transfer. Vol. 20, pp. 1241–1249. Pergamon Press 1977. Printed in Great Britain

LOCAL CONVECTIVE TRANSFER COEFFICIENTS IN A CHANNEL DOWNSTREAM OF A PARTIALLY CONSTRICTED INLET

E. M. SPARROW and J. P. KALEJS
Department of Mechanical Engineering, University of Minnesota, Minneapolis, Minnesota 55455, U.S.A.

(*Received* 3 *January* 1977 *and in revised form* 23 *February* 1977)

Abstract—Experiments have been performed to investigate the transfer coefficient distributions in the regions of flow separation, reattachment, and redevelopment along the walls of a channel whose inlet is partially constricted. The experiments were carried out for Reynolds numbers in the laminar range and utilized the naphthalene sublimation technique with air as the working fluid. The results revealed the presence of a new region of augmented transfer coefficients that is in addition to the zones of augmentation caused by the reattachment of the separated flow. The separated regions on the respective walls of the channel are of different length (i.e. short and long stalls) except at low Reynolds numbers and small constrictions. The new region of augmentation occurs on the wall of the channel that is washed by the short stall and is downstream of both the long and short stall reattachments. There is strong evidence that the new region of augmentation is caused by a vortex street shed from the tips of the constriction plates situated at the inlet.

NOMENCLATURE

- $\mathscr{D}$, diffusion coefficient;
- H, height of channel, Fig. 1;
- h, step height, Fig. 1;
- K, local mass-transfer coefficient based on $\Delta\rho = \rho_w - \rho_{bi}$;
- K_b, local mass-transfer coefficient based on $\Delta\rho = \rho_w - \rho_{bx}$;
- L^*, streamwise location of peak;
- $\dot{m}$, local mass-transfer rate;
- Re, Reynolds number, equation (1);
- Sc, Schmidt number;
- Sh, local Sherwood number, $K(2H)/\mathscr{D}$;
- Sh_b, local Sherwood number, $K_b(2H)/\mathscr{D}$;
- u_0, mean velocity in entrance slit;
- $\bar{u}$, mean velocity in channel;
- w_0, half opening of entrance slit, Fig. 1;
- x, streamwise coordinate.

Greek symbols

- ν, kinematic viscosity;
- ρ, concentration of naphthalene.

Subscripts

- bi, inlet bulk;
- bx, local bulk;
- w, wall.

INTRODUCTION

AN ABRUPT enlargement of the cross section of a tube or duct creates a downstream zone of flow separation. Beyond the separation zone, the flow reattaches to the duct wall and then redevelops. Experiments involving rectangular ducts [1–3] have shown that the streamwise length of the separation zone may be different along the individual walls of the duct. These experiments have dealt with two-dimensional enlargements (i.e. the spacing between only one pair of walls is enlarged) such that there is a backward facing step at each of the walls where the enlargement takes place. This flow configuration is termed a double backward facing step. The two separation zones, each situated downstream of its respective step, are referred to as long and short stalls in recognition of their different streamwise lengths [1]. The presence of stalls of different length has a marked effect on the heat-transfer characteristics at the duct walls downstream of the enlargement [2, 3].

The present research was undertaken to investigate the heat/mass transfer characteristics for flow and geometrical conditions that differ in a fundamental way from those of prior experiments involving double backward facing steps [1–3]. In particular, whereas all of the earlier experiments were performed for Reynolds numbers corresponding to turbulent duct flows, the present research was carried out at much lower Reynolds numbers, where duct flows are normally laminar. Furthermore, in all the prior experiments, the flow field upstream of the enlargement step was fully or partly hydrodynamically developed. In contrast, in the present study, the separating flow is drawn from the laboratory room through a slit bounded by sharp-edged plates. By this arrangement, it was intended to avoid the presence of upstream boundary layers which become free shear layers when separation occurs.

The present experiments were designed with the objective of closely approaching two-dimensional flow. To this end, a cross sectional aspect ratio of 20:1 was employed for the duct downstream of the enlargement. The cross sectional aspect ratios of the downstream ducts of [1–3] were substantially smaller, having values of <1:1, 3.2:1 and 4.7:1, and 1:1 respectively.

The research was carried out in the form of mass-transfer experiments via the naphthalene sublimation

technique. As will be described later, the implementation of this technique enabled highly localized measurements to be performed. This capability facilitated the resolution of the complex variations of the transfer coefficient along the duct walls. Other advantages of the naphthalene technique, compared with heat-transfer measurements, are that it is less susceptible to extraneous losses and facilitates the attainment of a uniform and well-defined boundary condition.

Measurements of the local mass-transfer rates were performed in the separation, reattachment, and redevelopment regions downstream of the enlargement steps on both principal walls of the duct. This information has been recast in dimensionless form in terms of the Sherwood number, which is the mass transfer counterpart of the Nusselt number. By means of the analogy between heat and mass transfer, these Sherwood numbers can be employed directly as Nusselt numbers for a fluid whose Prandtl number equals the Schmidt number ($=2.5$) of the mass-transfer experiments. The uniform wall concentration boundary condition of the experiments corresponds, via the analogy, to the case of uniform wall temperature.

The results of the present experiments have revealed phenomena and trends which were not observed in the earlier studies [1–3]. The most interesting of the new findings is a downstream maximum in the value of the transfer coefficient which is in addition to those at the points of reattachment of the long and short stalls. It occurs on the wall of the channel which is washed by the short stall, but is well downstream of the reattachment of that stall. This finding, as well as the other results, will be presented and discussed later.

A schematic diagram of the test section is presented in Fig. 1, with an inset at the lower right to show additional pertinent dimensions. As is seen there, air from the laboratory room passes through a slit formed by a pair of constriction plates and then emerges into a channel whose height H is greater than the slit opening $2w_0$. This enlargement in the cross section causes the flow to separate. The subsequent reattachment of the flow at the walls gives rise to an enclosed separation bubble behind each constriction plate. Within each bubble, there is a recirculating flow. After reattachment, the main flow begins to redevelop. The length of the channel is such that fully developed conditions were attained for the lower Reynolds numbers of the experiments, but not for the higher Reynolds numbers. Downstream of the channel, the flow emerges into a plenum chamber from which it is successively ducted to a rotometer, a blower, and to a roof-top exhaust.

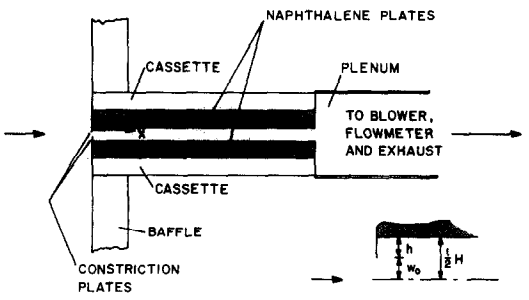

FIG. 1. Schematic diagram of the test section.

The two parameters that were varied during the course of the experiments are the constriction ratio h/w_0 and the Reynolds number. The former encompassed (nominal) values of 0.5, 1 and 2. The Reynolds number is defined here as

$$Re = \frac{u_0(4w_0)}{\nu} = \frac{\bar{u}(2H)}{\nu} \tag{1}$$

where u_0 and $\bar{u}$ are, respectively, the mean velocities in the entrance slit and in the channel. The first of the Reynolds numbers defined by equation (1) pertains to the flow through the constriction slit, whereas the second definition is that of a channel Reynolds number. In both cases, the characteristic dimension is twice the height of the passage, as for a parallel plate channel. The Reynolds number range of the experiments extended from about 190 to 1440.

THE EXPERIMENTS

Experimental apparatus

The flow path through the apparatus has already been discussed in the Introduction. The key components of the apparatus will now be described along with the most relevant aspects of the experimental procedure. A more detailed description is available in the thesis [4] on which this paper is based.

As seen in Fig. 1, the heart of the test section is the two naphthalene plates which serve as the principal walls of the channel where the separation, reattachment, and redevelopment take place. These plates were fabricated by a casting procedure which differs from that previously employed in our laboratory. In the past, naphthalene plates were cast and then removed from the mold prior to being incorporated into an appropriate test section. For the present research, the sometimes tenuous task of unmolding the naphthalene plates was circumvented. A mold was employed which not only served for the casting process, but which also became a part of the test section while still cradling its cast naphthalene plate. Two molds were employed, respectively for each of the two principal channel walls.

After casting, one of the walls of the mold was removed in order to expose the naphthalene surface which subsequently served as a bounding wall for the channel flow. In addition, a constriction plate was affixed to the forward part of the mold in order to form the test-section entrance slit as shown in Fig. 1. That part of the mold that cradles the naphthalene plate in the test section will be referred to as a cassette. As indicated in Fig. 1, each cassette served as a base for its respective naphthalene plate. In addition to the base, each cassette had side walls which bounded the spanwise breadth of the naphthalene plate.

The quality of the exposed naphthalene surface with respect to smoothness and flatness was such that no further machining was necessary. To prevent ex-

traneous sublimation from this surface prior to the data run, it was covered with a glass plate and the entire cassette wrapped in plastic. This package was left in the thermostatically controlled laboratory room for a minimum of 12 h in order to attain thermal equilibrium.

Only reagent grade naphthalene was used for the castings. New plates were cast for each experiment and the naphthalene was never re-used. A strict regime of cleanliness was maintained for all surfaces and implements which were exposed to the naphthalene. Further information about the molds, the cassettes, and the casting procedure are available in Chapter 3 of [4].

The channel height H was set with the aid of precisely machined spacers which rested on the side walls of the cassette and were secured in place by pins. The assembled test section consisted of the cassettes and their naphthalene plates, the spacers, and the entrance constriction plates. The upstream end of the test section was placed in a slot in a large baffle plate, with the upstream faces of the constriction plates aligned to be flush with the baffle. A plenum chamber situated downstream of the test section was used to collect the discharging flow and to duct it to the calibrated rotometer, from which it passed through a control and a cut-off valve and then to a blower. The ultimate exhaust was at the roof of the building so that the laboratory room is maintained free of naphthalene vapor.

A common channel height $H = 4.83$ mm (0.190 in) was used for all the experiments. Three entrance slit openings were employed, respectively $2w_0 = 1.65, 2.40$ and 3.17 mm (0.0650, 0.0945 and 0.125 in). These correspond to the constriction ratios

$$h/w_0 = 1.92, 1.01 \textit{ and } 0.52 \qquad (2)$$

which will be subsequently referred to in terms of their nominal values of 2, 1 and 0.5. The 96.5 mm (3.80 in) spanwise breadth of the channel provided a cross sectional aspect ratio of 20:1. The useful streamwise length of the channel was about 75 mm (3 in).

The constriction plates that formed the entrance slits were 0.61 mm (0.024 in) thick. The front face and the exposed edge of each plate were polished on a quartz lapping block, thereby providing well-defined sharp (in contrast to rounded) corners. The slip openings were spanwise uniform to within a few tenths of a percent or better.

Instrumentation and measurements

In order to determine local mass-transfer rates and transfer coefficients, it is necessary to measure the surface contours of the naphthalene plates both before and after a data run. The instrumentation employed to perform these measurements included a depth sensor with electronics to provide a voltage output, a printer-equipped digital voltmeter, and a coordinate table.

The naphthalene surface contours were measured with the cassette clamped to fixed reference blocks on the coordinate table and the depth sensor suspended above the table. Two calibrated feed controls producing horizontal motion of the coordinate table enabled precise positioning for both the streamwise and spanwise coordinates, respectively to within 0.0127 and 0.0254 mm (0.0005 and 0.001 in). The sensing head electronics allowed surface elevations as small as 0.00025 mm (10^{-5} in) to be resolved and recorded.

For each naphthalene plate, surface contours were measured along each of six parallel lines aligned in the streamwise direction. The parallel lines were spaced uniformly across the central portion of the breadth of the plate with a distance of 38.1 mm (1.5 in) separating the first and the sixth lines. Along each line, surface elevations were recorded at 42 points, with a higher density of points in the initial portion of the plate where separation and reattachment give rise to more rapid variations of the transfer rates. As will be discussed shortly, the results of the six contour measurements at each streamwise station were averaged to yield a final result for that station.

In addition to the aforementioned surface contour measurements, surface contours were also recorded along a pair of parallel lines on each of the side wall faces that are co-planar with the naphthalene plate. These side wall measurements are employed in the data reduction procedure to be described in the next section.

All told, measurements were made at 420 points on each plate, both before and after a data run. The measurement sequence for one plate lasted from 20 to 25 min. In addition to the surface contour and flow rate measurements that have already been mentioned, relevant pressure and temperature data were also recorded. The duration of the data runs and of the contour measurement sequences were carefully metered with a digital timer.

Data reduction

At any surface location, the mass transferred by sublimation during a data run can be determined by differencing the contour measurements made before and after the run and then applying suitable corrections. Three corrections were made. The first and second were for natural convection mass transfer that occurred during the time when the contour measurements were being performed and when the test section was being assembled. These natural convection corrections were determined from auxiliary *in situ* experiments [4]. The third correction was for changes in surface elevation inherent in removing and subsequently repositioning the cassette on the coordinate table. This positioning correction was accomplished by making use of the measured elevations on the side wall faces that are co-planar with the naphthalene plate [4]. These faces, being of metal, do not participate in the mass transfer process and, therefore, any measured changes in their elevation are due to positioning.

The local changes in surface elevation, corrected as discussed above, may be termed the sublimation depth $\delta(x, y)$. A sublimation depth $\Delta(x)$ representative of a

given streamwise station x was evaluated as

$$\Delta(x) = (1/6)\sum_{i=1}^{6}\delta(x, y_i) \tag{3}$$

where the average encompasses the aforementioned six spanwise measurement locations. Except for one set of operating conditions, the individual inputs $\delta(x, y_i)$ were generally within 5% of the mean value, $\Delta(x)$. The local mass-transfer rate at x was then computed from

$$\dot{m}(x) = \rho_s\Delta(x)/t_0 \tag{4}$$

where t_0 is the duration time of the data run and ρ_s is the density of the solid naphthalene.

A local mass-transfer coefficient may be defined as

$$K(x) = \dot{m}(x)/\Delta\rho \tag{5}$$

where $\Delta\rho$ is the naphthalene vapor concentration difference. Two concentration differences were considered here

$$\Delta\rho = \rho_w - \rho_{bi}, \quad \Delta\rho = \rho_w - \rho_{bx} \tag{6}$$

where ρ_w is the concentration of naphthalene vapor at the wall, and ρ_{bi} and ρ_{bx} are, respectively, the inlet and local bulk concentrations. If it is noted that ρ_w is constant along the channel wall and that $\rho_{bi} = 0$, then the first definition reduces to $\Delta\rho = \rho_w$ = constant. Consequently, as is evident from equation (5), $K(x)$ is a true reflection of the streamwise variation of the mass-transfer rate. On the other hand, the second definition yields a $\Delta\rho$ which is a function of x so that $K(x)$ responds to both $\dot{m}(x)$ and $\Delta\rho(x)$.

The first definition of $\Delta\rho$ was selected for the primary presentation of results because it promotes greater fidelity between $K(x)$ and $\dot{m}$. Representative results based on the second definition will also be presented. For concreteness, we write

$$K = \dot{m}/\rho_w, \quad K_b = \dot{m}/(\rho_w - \rho_{bx}). \tag{7}$$

Values of ρ_w were computed by employing the Sogin relation [5] for the vapor pressure of naphthalene in conjunction with the perfect gas law. The local bulk concentration was obtained from

$$\rho_{bx} = \rho_{bi} + \dot{M}(x)/\dot{Q} \tag{8}$$

where $\dot{M}(x)$ is the overall rate of mass transfer from $x = 0$ to $x = x$ from both of the channel walls, and $\dot{Q}$ is the volume flow through the test section.

The local Sherwood number is the dimensionless counterpart of the local mass-transfer coefficient. It is defined here as

$$Sh = K(2H)/\mathscr{D}, \quad Sh_b = K_b(2H)/\mathscr{D} \tag{9}$$

where $2H$ is the hydraulic diameter of a parallel plate channel and $\mathscr{D}$, the naphthalene–air diffusion coefficient, was evaluated via the Schmidt number $Sc = \nu/\mathscr{D}$ with $Sc = 2.5$ and ν as the kinematic viscosity of air.

LOCAL TRANSFER COEFFICIENTS

The measured distributions of the local transfer coefficients along the bounding walls of the channel are presented in Figs. 2–4, respectively for constriction ratios h/w_0 of 0.5, 1 and 2. In the figures, the local Sherwood number is plotted as a function of the dimensionless streamwise coordinate x/H, where x is measured from the downstream face of the constriction plates. The Sherwood number appearing in these figures is based on the concentration difference $(\rho_w - \rho_{bi})$, which is a constant for each data run.

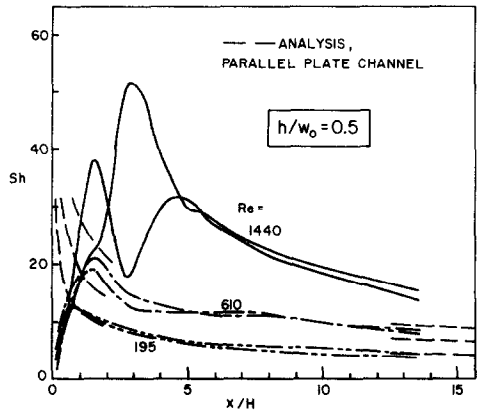

FIG. 2. Distributions of the local Sherwood number along the channel walls, constriction ratio $h/w_0 = 0.5$.

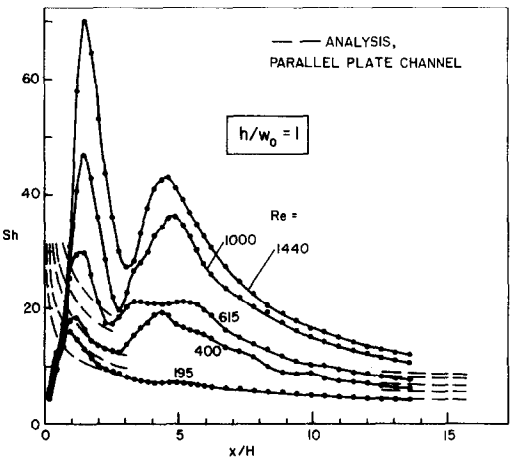

FIG. 3(a). Distributions of the local Sherwood number along the short-stall wall, constriction ratio $h/w_0 = 1$.

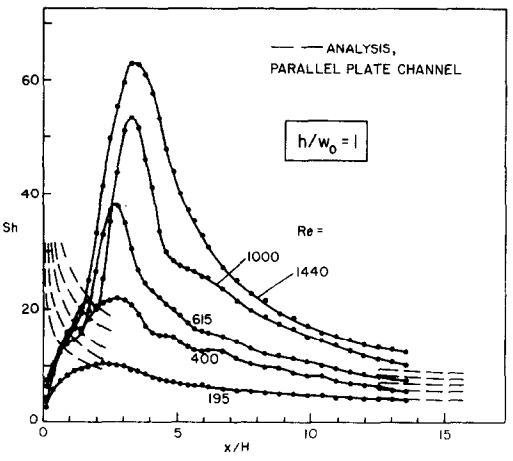

FIG. 3(b). Distributions of the local Sherwood number along the long-stall wall, constriction ratio $h/w_0 = 1$.

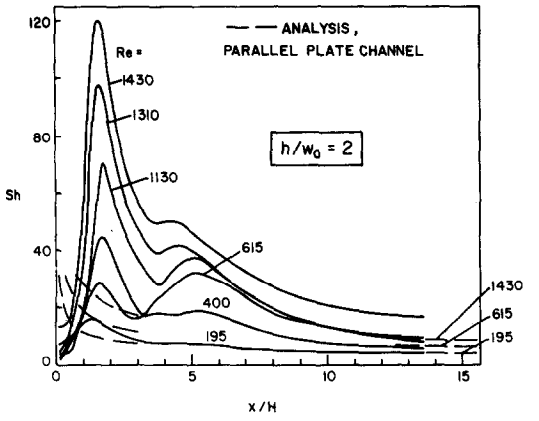

FIG. 4(a). Distributions of the local Sherwood number along the short-stall wall, constriction ratio $h/w_0 = 2$.

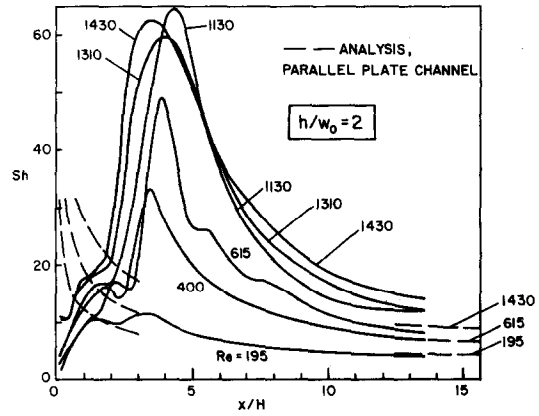

FIG. 4(b). Distributions of the local Sherwood number along the long-stall wall, constriction ratio $h/w_0 = 2$.

Therefore, the streamwise variation of the Sherwood number is a direct reflection of the variation of the mass-transfer rate. The results correspond to a Schmidt number of 2.5.

In each figure, the curves are parameterized by the Reynolds number, with the number of *Re* values and their magnitudes being selected to facilitate a clear description of the results for each constriction ratio. The largest Reynolds number consistent with the available instrumentation is about 1440. For the case of least constriction ($h/w_0 = 0.5$), where data were taken at three Reynolds numbers, the results for both walls of the channel were plotted in the same figure (i.e. Fig. 2). For the other cases, more Reynolds numbers were employed and this necessitated that the results for each channel wall be plotted separately. Therefore, Figs. 3 and 4 have (a) and (b) parts. The (a) part corresponds to the short-stall wall and the (b) part to the long-stall wall.

The data points are shown in Figs. 3(a) and (b), but are omitted from the other figures to avoid crowding and confusion. Also appearing in the figures are dashed curves depicting Sherwood number results for $Sc = 2.5$ from a finite difference solution for simultaneously developing laminar velocity and concentration distributions in a parallel plate channel without constriction. Only the initial and final portions of these curves are shown in the interests of clarity.

Short stall, long stall, and tertiary maxima

Inspection of Figs. 2–4 reveals a complex pattern of trends and variations in the transfer coefficient distributions, with both the constriction ratio and the Reynolds number playing important roles. Before the specific trends are identified and discussed, certain general characteristics will be described.

The presence of the inlet constriction gives rise to very low values of the transfer coefficient immediately downstream of the constriction plates, but the coefficient increases rapidly with increasing downstream distance and ultimately attains a maximum at the point where the separated flow reattaches to the wall. For most of the operating conditions of the present experiments, the reattachment occurs considerably farther downstream on one wall than on the other, as reflected by the distribution curves. Therefore, in spite of the significant differences in the flow configuration and in the Reynolds number range, the short and long stall phenomenon that was encountered in [1–3] is also in evidence here.

Downstream of the long stall peak, the transfer coefficients decrease monotonically. On the other hand, the coefficients do not decrease monotonically downstream of the short stall peak. Instead, the decrease is arrested and the coefficients increase once again, attain a maximum, and then begin a steady decrease. This additional maximum will be termed the tertiary maximum. It has not been observed in any of the previous investigations of flow downstream of a double backward facing step, all of which were carried out at Reynolds numbers corresponding to turbulent duct flow. The discovery of the tertiary maximum is, therefore, one of the main outcomes of the present study. Possible causes of the tertiary maximum will be discussed later.

From a careful study of Figs. 2–4, it may be observed that the tertiary maximum undergoes an evolution as the Reynolds number increases, with the nature of the evolution being dependent on the constriction ratio. In no case can a tertiary maximum be identified at the lowest Reynolds number of the experiments, $Re = 195$. For the minimum constriction, $h/w_0 = 0.5$, the evolution is slow and only a trace of a tertiary maximum can be seen at $Re = 610$. A full-blown tertiary peak exists at $Re = 1440$. For the intermediate constriction, $h/w_0 = 1$, the evolution process is more rapid. A tertiary peak is already strongly in evidence at $Re = 400$, and it continues to grow and remain distinct as the Reynolds number increases.

The process of evolution appears to be even more rapid at the largest constriction, $h/w_0 = 2$, so that a greater portion of the life history of the tertiary peak is exposed in the given Reynolds number range. The birth and initial growth of the peak occur as before. However, at higher Reynolds numbers, its further growth appears to be stunted, and it tends to become a

diminishing shoulder on the downslope of the short stall peak.

The short stall and long stall maxima also exhibit an evolution as a function of the Reynolds number. In general, these peaks grow taller with increasing Reynolds number. The only exception to this trend is for $h/w_0 = 2$, where the growth of the long stall peak is arrested within the same range of Reynolds numbers where the tertiary peak diminishes. At the smallest constriction ratio and Reynolds number, separate short and long stalls are not in evidence, thereby suggesting that threshold values of these parameters have to be exceeded before distinct stalls occur.

The streamwise locations of the short and long stall maxima will be presented in a later figure (Fig. 5) in order to facilitate their comparison with literature values. The tertiary maximum is, in all cases, located downstream of the long stall maximum.

The transfer coefficients at the three maxima are generally much larger than those at corresponding locations in a conventional laminar channel flow. To obtain an indication of the degree of augmentation, each of the measured peak transfer coefficients may be ratioed with the analytical value for the channel flow at the same x/H and Re. For $h/w_0 = 0.5$, the maximum augmentation occurs at the highest Reynolds number, the augmentation ratios being 1.6, 2.9 and 2.2 respectively for the short stall, long stall, and tertiary peaks. The comparable factors for $h/w_0 = 1$ are 3.0, 3.9 and 3.0. For $h/w_0 = 2$, the augmentation ratios for the short stall and tertiary peaks increase more or less monotonically with Reynolds number to values of 5.2 and 3.5 respectively. The augmentation ratio for the long stall peak reaches a maximum of 4.9 at $Re = 1130$ and declines thereafter.

The foregoing results indicate that the extent of the augmentation is appreciable. In general, the largest augmentations occur for the greatest constriction and at the larger Reynolds numbers.

Other aspects of the results

Before leaving Figs. 2–4, there are other aspects of the results that warrant discussion. One of these is the behavior of the transfer coefficients at streamwise locations downstream of the maxima. There is a clear trend for the coefficients on both walls to approach those for a conventional laminar channel flow (dashed lines). At the lower Reynolds numbers, there is near coincidence of the experimental results and the dashed lines. These findings suggest that laminar conditions are maintained in the channel even in the presence of the flow separation and reattachment.

Another interesting feature of the curves of Figs. 2–4 is the presence of a variety of minor peaks and shoulders. For instance, such peaks and shoulders can be observed at locations upstream of the long stall maximum for all the curves of Fig. 4(b). Another such shoulder forms the forward edge of the tertiary peak for $Re = 615$ in Fig. 3(a). These peaks and shoulders are believed to be the result of temporary and short-lived shifts of the flow pattern from one wall to the other during the course of the data run. Therefore, each such peak or shoulder corresponds to the temporary presence of one of the major peaks on the wall opposite to that where it normally resides. Thus, it can be easily verified that the aforementioned shoulder in Fig. 3(a) spans the same range of x/H as does the long stall maximum of Fig. 3(b). A similar verification can be made for all of the other peaks and shoulders.

Careful examination of a large number of replication data runs indicated that from run to run, there was not a consistent preference of the short stall for one wall of the channel and of the long stall for the other wall. However, for any given data run, the flow pattern was essentially fixed except for the short-lived shifts noted in the foregoing.

Direct numerical comparisons between the transfer coefficients of Figs. 2–4 and those of the published literature are not appropriate because of major differences in operating conditions. The only previously published local transfer coefficient distributions for a two-dimensional, double backward facing step are those of [2] for heat transfer downstream of a sudden enlargement. However, the Reynolds numbers of those experiments are more than two orders of magnitude greater than the Reynolds numbers of the present investigation. As already noted, tertiary peaks have not been previously encountered. In addition, there are differences between the shapes of the short stall and long stall peaks of Figs. 2–4 and those of [2]. The peaks encountered here are quite symmetric, whereas there is a pronounced skewing in the peaks of [2], with a slower decay on the downstream side.

The streamwise locations of the short and long stall maxima can be read from Figs. 2–4 and compared with information in the literature. An extensive investigation of the reattachment of the separated flow downstream of a two-dimensional sudden enlargement was performed in [1] using visualization techniques. Those studies encompassed the Reynolds number range from 20 000 to 50 000. At a given h/w_0, the reattachment lengths of [1] were found to be independent of the Reynolds number, but the data exhibited a rather broad scatter band.

In Fig. 5, the streamwise locations of the peaks, denoted by L^*, are plotted as a function of the

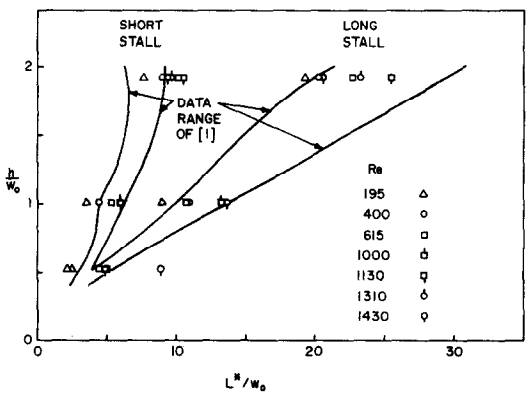

FIG. 5. Reattachment lengths for the short and long stalls.

constriction ratio h/w_0, with the various Reynolds numbers being identified by different data symbols. The lines appearing in the figure represent the data range of [1]. The figure shows that the present reattachment lengths fall within or adjacent to the data brackets of [1]. This finding is noteworthy in view of the large difference in the Reynolds number ranges of the two investigations and the probability that the flow regimes were different. Another seemingly relevant difference is the presence of established upstream boundary layers in [1] (which become shear layers after separation) as contrasted to the absence of such boundary layers in the present flow configuration. On the basis of the comparison shown in Fig. 5, the reattachment length appears not to be very sensitive to these factors. A close inspection of the data in Fig. 5 indicates an overall trend for L^* to increase with Reynolds number, but the trend is not consistently monotonic at the higher Reynolds numbers.

Transfer coefficients for duct flows are frequently based on the wall-to-bulk temperature (or concentration) difference as defined in the second of equations (6). Such a coefficient is convenient to use in the thermally developed regime because it is a constant, but it has no special merits in the entrance region. For completeness, a limited presentation of results is made in Fig. 6 in terms of the Sherwood number Sh_b based on the wall-to-bulk concentration difference. In that figure, Sh_b is plotted as a function of x/H for the Reynolds number extremes of 195 and 1440 for the constriction ratio $h/w_0 = 1$. The figure includes results for both walls.

A comparison of Figs. 3 and 6 reveals that the essential trends are not affected by the alternate definition of the Sherwood number. Furthermore, for small values of x/H (up to the short stall peak), Sh_b Sh. Thereafter, the deviations between Sh_b and Sh increase steadily. In particular, the downstream drop-off of Sh_b is slower than that of Sh, which gives rise to a modest skewing of the long stall and tertiary peaks. At the last measuring station, Sh_b is larger than Sh by 25 and 60%, respectively for $Re = 195$ and 1440.

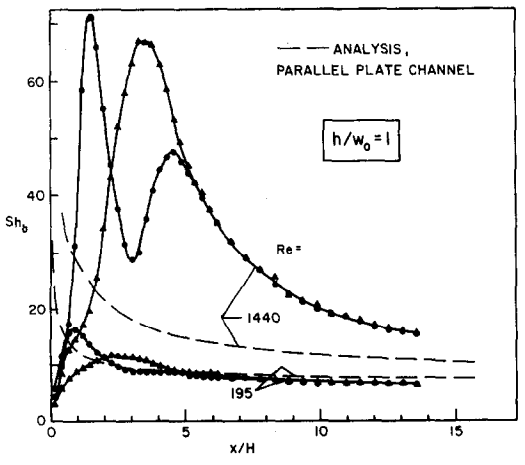

FIG. 6. Representative Sherwood number distributions based on the wall-to-bulk concentration difference.

THE TERTIARY MAXIMUM

The presence of the tertiary maximum in the transfer coefficient distributions is a finding that is unique to the present laminar-range Reynolds number experiments. It is, therefore, appropriate to seek possible causes for the existence of this maximum. A number of potential causal phenomena were considered by the authors, as will be discussed in the paragraphs that follow.

The most likely cause of the tertiary maximum is a vortex street that is shed from the tips of the constriction plates. In [6], it was found by flow visualization that for Reynolds numbers above a threshold value, a vortex street was shed from the sharp edges of a two-dimensional slit in an orifice plate. Whereas the strength of the shed vortices presumably increases with Reynolds number, the streamwise life span of the vortex street decreases. The demise of the vortex street appears to be due to mutual annihilation of interacting vortices. Furthermore, the geometrical characteristics of the vortex street appear to scale with the slit opening, so that the streamwise life span of the street diminishes as the slit opening decreases. It was also found that the vortex street follows the curved flight path of the jet that issues from the orifice and that a street of sufficient life span migrates to one of the side walls of the test section.

All of the essential characteristics of the tertiary maximum are well correlated with those of the shed vortex street. These include the absence of the maximum at low Reynolds numbers, its growth with increasing Reynolds number, the acceleration of its life history at greater constrictions, and its tendency to disappear at higher Reynolds numbers for the most constricted inlet. The positioning of the tertiary peak downstream of the short stall reattachment is also consistent with the flight path of the vortex street. Finally, the absence of the tertiary peak from the prior high Reynolds number experiments [1–3] is consistent with the rapid breakup of the vortex street at these Reynolds numbers. Aside from the Reynolds number, another possible reason for the absence of shed vortices in the prior experiments is that the separating flow was supplied via an upstream duct or nozzle rather than a sharp edge orifice.

Although it is highly likely that the shed vortex street is the cause of the tertiary maximum, it is interesting to briefly air some of the other causes considered by the authors. One of these is the conjecture that the tertiary maximum is due to a transition from laminar to turbulent flow beyond the short stall reattachment. If the tertiary maximum were to represent a zone of transitional or turbulent flow, then a subsequent laminarization would have to occur in order to fulfill the experimental fact that the downstream flow is laminar.

Another conjecture is that there is a zone of separation adjacent to the short-stall wall, downstream of the short stall reattachment. The presence of such a separation bubble might be made plausible by noting that there is a pressure recovery downstream

of the constricted inlet, so that the flow must press forward against an adverse pressure gradient. Once the short stall has reattached, the flow adjacent to the short-stall wall must contend with both wall friction and an adverse pressure gradient and may, therefore, separate.

The conjectures that were outlined in the two prior paragraphs do not explain all of the observed characteristics of the tertiary maximum. It is believed that they are less likely to be the cause of this maximum than is the shed vortex street.

Auxiliary experiments were performed to demonstrate that the tertiary maximum is not an extraneous phenomenon caused by surface irregularities resulting from excessive local sublimation. In these experiments, the duration time of each data run was reduced so that the maximum change in surface contour was 0.02 mm (0.0008 in). These experiments yielded results identical to those obtained from data runs where the surface contour changes were as much as 0.1 mm (0.004 in).

CONCLUDING REMARKS

The major novel finding of the present laminar-range experiments is the discovery of a new region of augmented transfer coefficients downstream of a double backward facing step. This region is in addition to the zones of augmentation caused by the reattachment of the separated flow. The two separated regions, each situated downstream of its respective step, are of different streamwise length (i.e. short and long stalls) except at low Reynolds numbers and small constrictions. The new region of augmentation occurs on the wall of the channel washed by the short stall and is downstream of both the short and long stall reattachments. The short and long stall phenomenon has been encountered previously in turbulent-range experiments, but the third region of augmentation (i.e. the tertiary maximum) has not been observed before.

The tertiary maximum does not exist at the lowest Reynolds number of the experiments ($Re \sim 200$) and evolves with increasing Reynolds number. The rate of evolution is more rapid when the constriction is large. At the largest constriction ($h/w_0 = 2$), the growth of the tertiary maximum is arrested at Reynolds numbers beyond 1000, and it diminishes thereafter. There is strong evidence that the tertiary maximum is caused by a vortex street shed from the tips of the constriction plates situated at the inlet of the channel.

At the short stall, long stall, and tertiary peaks, the transfer coefficients are substantially larger than those at corresponding locations in a conventional laminar channel flow. Downstream of the peaks, the transfer coefficients approach the channel flow values. The streamwise locations of the short and long stall peaks are in the same range as those of the prior turbulent flow studies.

Acknowledgement—This research was performed under the auspices of NSF Grant ENG75-03221.

REFERENCES

1. D. E. Abbot and S. J. Kline, Experimental investigation of subsonic flow over single and double backward facing steps, *J. Basic Engng* **84**, 317–325 (1962).
2. E. G. Filetti and W. M. Kays, Heat transfer in separated, reattached, and redevelopment regions behind a double step at entrance to a flat duct, *J. Heat Transfer* **89C**, 163–168 (1967).
3. N. Seki, S. Fukusako and T. Hirata, Effect of stall length on heat transfer in reattached region behind a double step at entrance to an enlarged flat duct, *Int. J. Heat Mass Transfer* **19**, 700–702 (1976).
4. J. P. Kalejs, Local transfer coefficients due to separation downstream of a double backward facing step, Thesis, Department of Mechanical Engineering, University of Minnesota, Minneapolis, Minnesota (1976).
5. H. H. Sogin, Sublimation from disks to air streams flowing normal to their surfaces, *Trans. Am. Soc. Mech. Engrs* **80**, 61–71 (1958).
6. G. S. Beavers and T. A. Wilson, Vortex growth in jets, *J. Fluid Mech.* **44**, 97–112 (1970).

COEFFICIENTS LOCAUX DE CONVECTION DANS UN CANAL EN AVAL D'UNE ENTREE PARTIELLEMENT RESSERREE

Résumé—Des expériences ont été faites pour étudier les distributions du coefficient de convection dans les régions de séparation, de réattachement et de redéveloppement le long des parois d'un canal dont l'entrée est partiellement resserrée. Les nombres de Reynolds correspondent au domaine laminaire et on a utilisé la méthode de sublimation du naphtalène avec l'air comme fluide de travail. Les résultats revèlent la présence d'une région nouvelle d'augmentation des coefficients de transfert, en addition des zones d'augmentation provoquées par le réattachement de l'écoulement décollé. Les régions de séparation sur les parois respectives du canal sont de longueurs différentes sauf pour les faibles nombres de Reynolds et les petites constrictions. La nouvelle région d'augmentation se produit sur la paroi du canal qui est balayée par la région la plus courte et elle est située en aval des deux plages de réattachement. A l'évidence, la nouvelle région d'augmentation est provoquée par une allée de tourbillons issue des bords des plaques de constriction situées à l'entrée.

ÖRTLICHE, KONVEKTIVE ÜBERGANGSKOEFFIZIENTEN IN EINEM KANAL HINTER EINEM TEILWEISE VERENGTEN EINLAUF

Zusammenfassung—Es wurde der Verlauf des Übergangskoeffizienten im Bereich der Strömungsablösung, des Wiederanlegens und der Neuausbildung der Strömung entlang den Wänden eines Kanals, dessen Einlauf teilweise verengt ist, experimentell untersucht. Die Versuche wurden mit Reynolds-Zahlen im laminaren Bereich durchgeführt; es wurde die Naphthalin-Sublimations-Methode mit Luft als Arbeitsmittel verwendet. Die Ergebnisse zeigten einen neuen Bereich erhöhter Übergangskoeffizienten, zusätzlich zu den

Erhöhungszonen im Bereich des Wiederanlegens der abgelösten Strömung. Die getrennten Bereiche weisen an den verschiedenen Kanalwänden unterschiedliche Längen auf, ausgenommen bei niedrigen Reynolds–Zahlen und kleinen Verengungen. Die neue Zone erhöhten Wärmeübergangs tritt an der Kanalwand auf, an der sich die Strömung früher wieder anlegt und befindet sich stromabwärts von beiden Wiederanlegungszonen. Die neue Zone erhöhten Wärmeübergangs ist offensichtlich auf eine, von den Kanten der am Einlauf angebrachten Verengungsplatten ausgehende Wirbelstraße zurückzuführen.

КОЭФФИЦИЕНТЫ ЛОКАЛЬНОГО КОНВЕКТИВНОГО ПЕРЕНОСА В КАНАЛЕ ЗА ЧАСТИЧНО СУЖЕННЫМ УЧАСТКОМ НА ВХОДЕ

Аннотация — Экспериментально исследовалось распределение коэффициентов переноса в области отрыва, присоединения и повторного развития потока вдоль стен с частично суженным участком на входе. Опыты проводились при числах Рейнольдса, соответствующих ламинарному течению. Использовался метод сублимации нафталина в воздухе. Результаты показали наличие новой области с более высокими коэффициентами переноса, чем в зоне присоединения сорванного потока. Длина зон отрыва на соответствующих стенках канала различна (т. е. имеют место короткие и длинные отрывные зоны), за исключением течения с низкими числами Рейнольдса и небольших сужений. Новая область интенсивного переноса образуется на стенке канала, омываемой короткой отрывной зоной, и она располагается за областью присоединения потока. Имеются веские доказательства в пользу того, что новая область интенсивного переноса вызывается вихревой дорожкой, срывающейся с пластин, суживающих вход.